

Updating Circuit Theory: The Signal Link

By Ian Darney

Here, we define a circuit model that can simulate all the mechanisms involved in the coupling of electromagnetic interference, and then the accuracy of the simulation is demonstrated by comparing it with the response of a test rig.

Test rig

The basic test rig consists of a length of copper pipe installed round the walls of a room, with a wood batten fixed along its length. Then the cable under test was installed along the length of the batten. Figure 1 shows a cross section of the assembly.

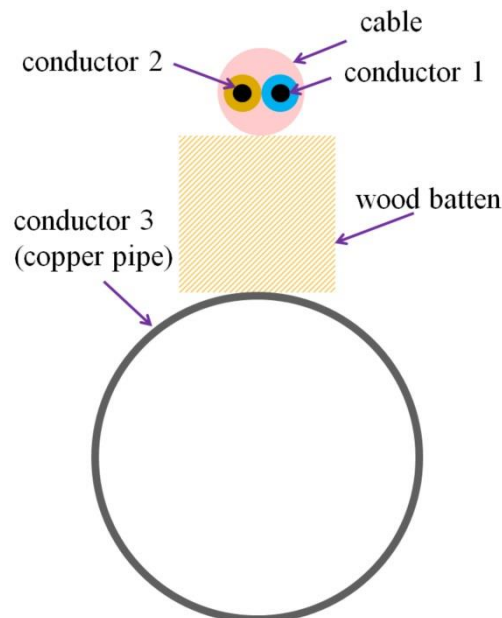


Figure 1 Cross-section of test rig

The method of measurement is illustrated by the setup of Figure 2. The copper pipe can represent the conducting structure of a vehicle, aircraft or spacecraft.

One of the cable conductors was used to send a signal whilst the other was assigned to carry the return current. The terminals at the far end were shorted together. A signal generator was used to provide a variable frequency voltage source V_{in} at the near end, and the peak-to-peak amplitude was measured by channel 1 of the oscilloscope.

From Figure 2:

$$V_{ch1} = \frac{50}{50 + 41} \cdot V_{in} \quad (1)$$

Since the source impedance was less than 10 ohm, the loading effect of the assembly under review had minimal effect on the load presented to the signal generator.

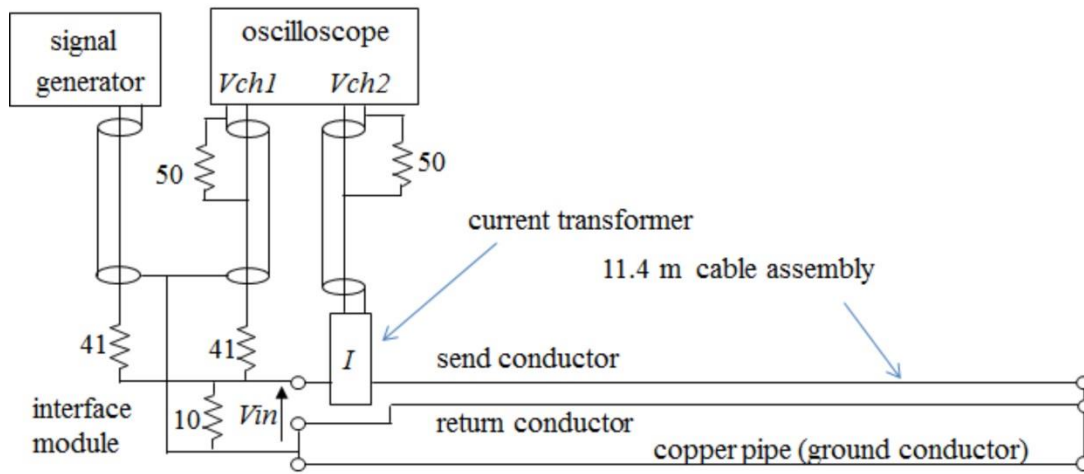
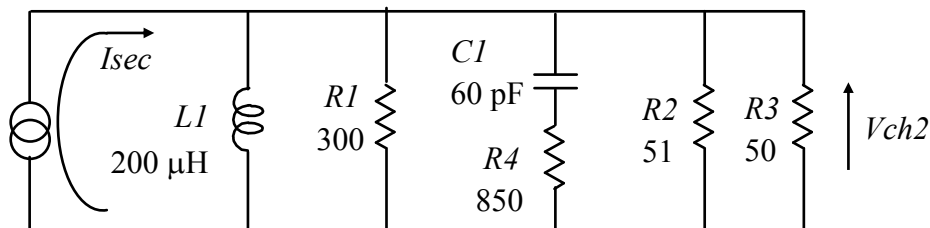


Figure 2 Setup to characterise the test rig

Current in the send conductor I_{prim} flows through the core of the current transformer and the output of the ten-turn secondary is monitored by V_{ch2} of the oscilloscope. The relationship between these two parameters is defined by the circuit model of Figure 3. The method of deriving this model is described in the article ‘The current monitor transformer’ that’s part of this series.

At any particular frequency there is a one-to-one correlation between the amplitude of the input current and the amplitude of the output voltage. Conversely, if the amplitude of V_{ch2} is known, then the amplitude of I_{prim} can be calculated. It is simply a matter of invoking the equations of Circuit Theory.



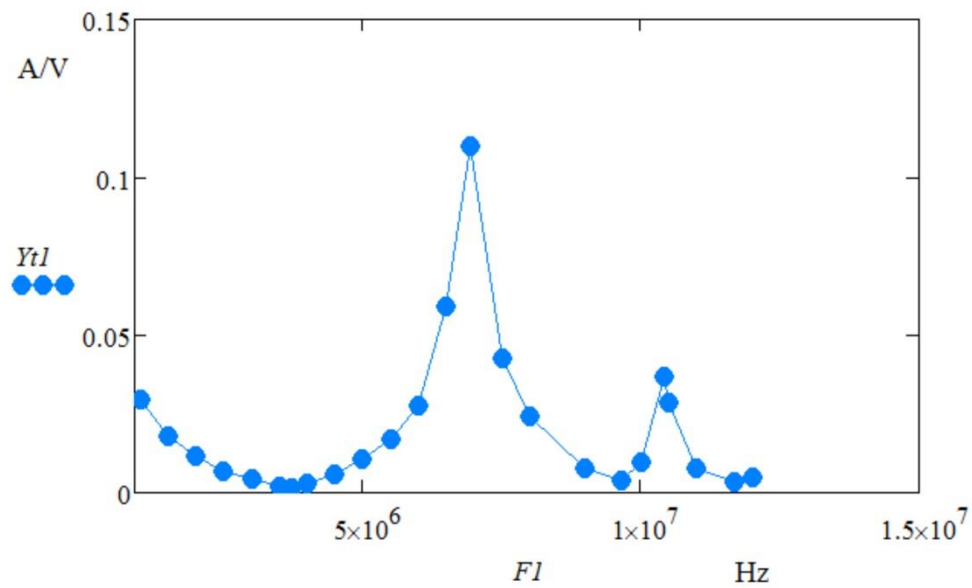
$$I_{prim} = I_{sec} \cdot Turns$$

Figure 3 Circuit model of current transformer

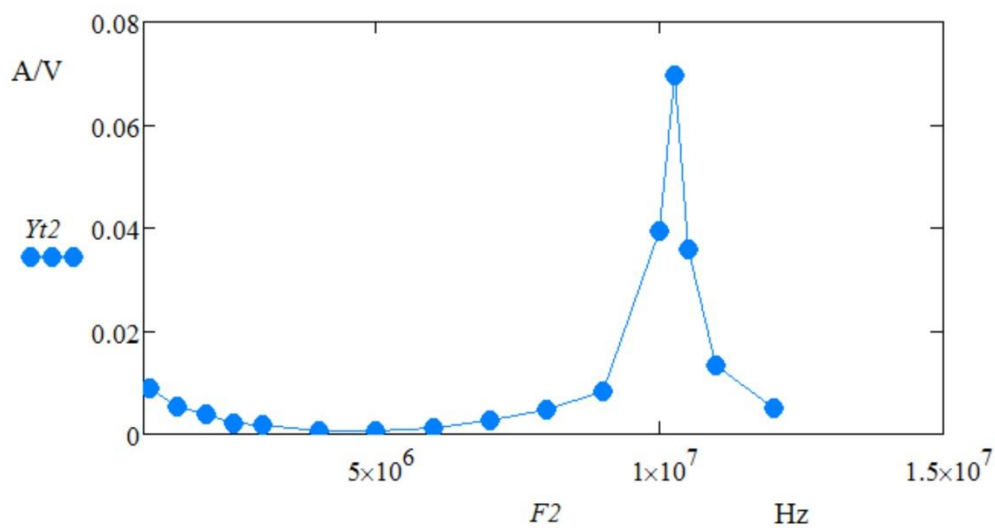
Calculating the ratio of I_{prim} to V_{in} gives a value for the admittance:

$$Y_t = \frac{I_{prim}}{V_{chl}} \quad (2)$$

Carrying out this measurement over a set of spot frequencies gave the graph of Figure 4a. Then the current transformer was clamped round both conductor and the test repeated, to give the response illustrated by Figure 4b.



a



b

Figure 4 Frequency response tests of test rig
a Admittance of differential-mode loop
b Transfer admittance of common-mode loop

Initial circuit model

The next step in the design process was to create a model that replicates these test results. The article ‘The three conductor model’, also part of the series, derives the Triple-T model of lumped parameters illustrated by Figure 5a. Initial values for the components were derived from the geometry of the assembly.

From Figure 1:

$r11 = r22 = 0.61$ mm	radii of send and return conductors
$r33 = 7.5$ mm	radius of copper pipe
$r12 = 2.45$ mm	separation between send and return conductors
$r13 = r23 = 23$ mm	separation of conductors from pipe.

The length of the test rig was measured to be: $l = 11.4$ m

The initial values of the inductors were:

$$\begin{aligned}
 Lc1 &= \frac{\mu_o \cdot \mu_r \cdot l}{2 \cdot \pi} \cdot \ln\left(\frac{r12 \cdot r13}{r11 \cdot r23}\right) = 3.17 \times 10^{-6} \text{ H} \\
 Lc2 &= \frac{\mu_o \cdot \mu_r \cdot l}{2 \cdot \pi} \cdot \ln\left(\frac{r12 \cdot r23}{r22 \cdot r13}\right) = 3.17 \times 10^{-6} \text{ H} \\
 Lc3 &= \frac{\mu_o \cdot \mu_r \cdot l}{2 \cdot \pi} \cdot \ln\left(\frac{r13 \cdot r23}{r33 \cdot r12}\right) = 7.66 \times 10^{-6} \text{ H}
 \end{aligned} \tag{3}$$

The initial values of the capacitors were

$$\begin{aligned}
 Cc1 &= \frac{2 \cdot \pi \cdot \epsilon_o \cdot \epsilon_r \cdot l}{\ln\left(\frac{r12 \cdot r13}{r11 \cdot r23}\right)} = 4.56 \times 10^{-10} \text{ Farad} \\
 Cc2 &= \frac{2 \cdot \pi \cdot \epsilon_o \cdot \epsilon_r \cdot l}{\ln\left(\frac{r12 \cdot r23}{r22 \cdot r13}\right)} = 4.56 \times 10^{-10} \text{ Farad} \\
 Cc3 &= \frac{2 \cdot \pi \cdot \epsilon_o \cdot \epsilon_r \cdot l}{\ln\left(\frac{r13 \cdot r23}{r33 \cdot r12}\right)} = 1.89 \times 10^{-10} \text{ Farad}
 \end{aligned} \tag{4}$$

Resistances of the conductors were assumed to be

$$\begin{aligned}
 Rc1 &= 0.17 \text{ ohm} \\
 Rc2 &= 0.17 \text{ ohm} \\
 Rc3 &= 0.005 \text{ ohm}
 \end{aligned} \tag{5}$$

Textbook analysis of transmission lines leads to the conclusion that, unless the line is terminated by its characteristic impedance, reflections will occur at that termination. This means that there will be partial currents flowing in both directions in all three conductors.

If it is assumed that the signals are oscillatory, then a circuit model can be created to simulate the action of the line. Each conductor is represented as a T-network of impedances, where the value of each impedance is a function of the R, L, and C values of the lumped-parameter model. The article ‘The Transformation Equations’ derives a set of equations that define the relationship between the two models.

This relationship can also be applied to the three-conductor configuration, as illustrated by comparing Figure 5b with Figure 5a.

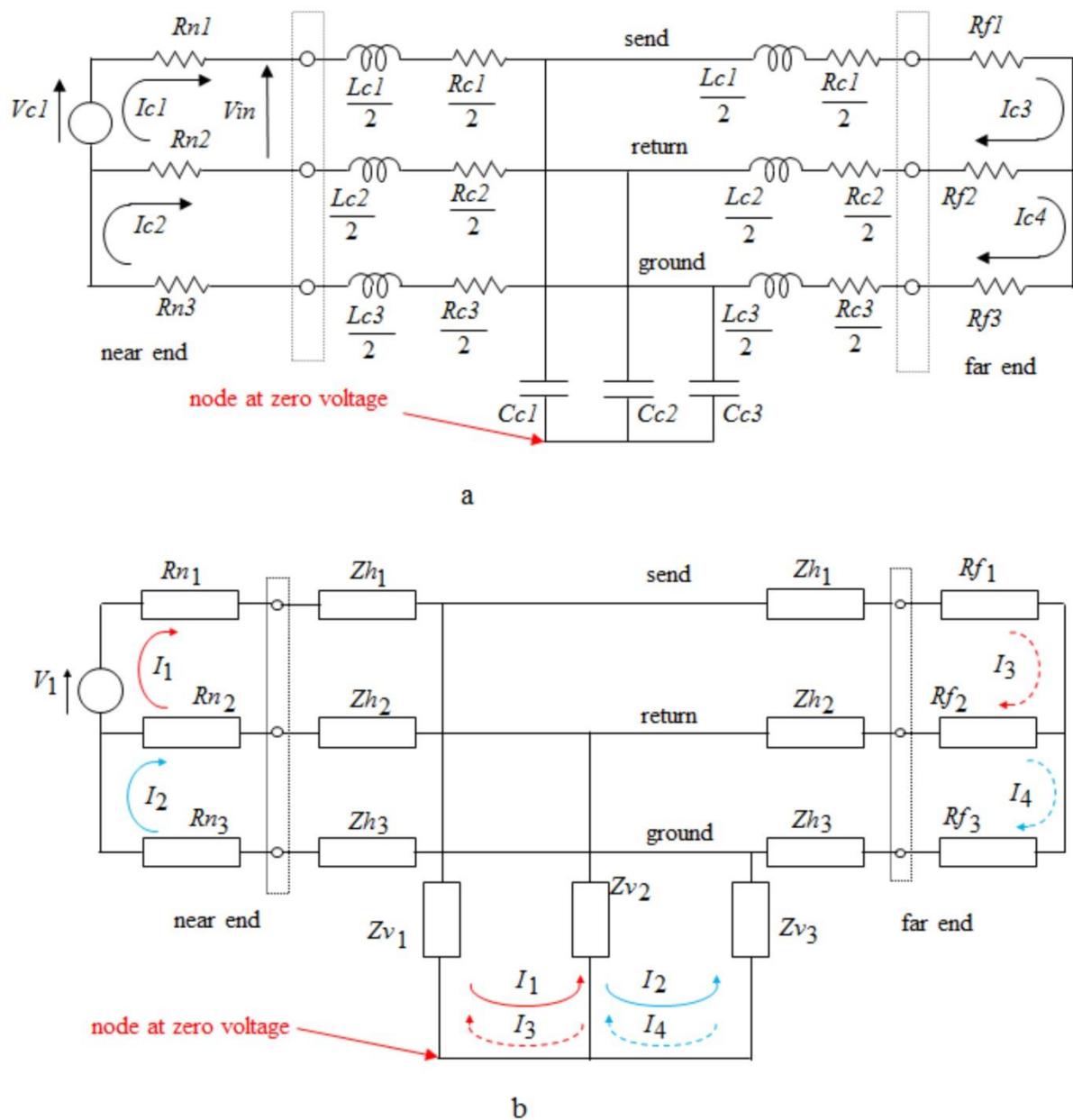


Figure 5 Triple-T models of the test rig
a Lumped parameter model
b Distributed-parameter model

The function $Zbranch(f)$ at the top of the Mathcad worksheet of Figure 6 invokes this relationship to assign values to the impedances Zh_i and Zv_i , where the character 'i' identifies the associated conductor. The output of this function is a pair of vectors containing these impedance values at the frequency f .

The function $Zloop(f)$ picks up these values and uses them to compile a set of loop impedances. Each loop impedance is the sum of the branch impedances along the path of a particular current flow in the circuit of Figure 5b. For example, $Z11$ is the sum of Rn_1 , Zh_1 , Zv_1 , Zv_2 , Zh_2 and Rn_2 , since that is the path followed by I_1 . Since mesh analysis is used, it is assumed that many currents can flow in any particular impedance. Hence $Z12$ is the sum of Rn_2 , Zv_1 and Zv_2 , since these are the impedances shared by I_1 and I_2 . The minus sign exists because I_1 and I_2 are flowing in opposite directions in these components.

The final action of the subroutine of $Zloop(f)$ is to assemble these loop parameters into a four-by-four array. There are only ten independent loop parameters, since $Z12 = Z21$, $Z13 = Z31$, etc. This means that the array is symmetrical. This array is the output of the function $Zloop(f)$.

The next action of the worksheet is to set up the control variable i and use it to define the frequency vector F_i . The voltage vector V assumes that the voltage source is in loop 1, that its amplitude is 1 Volt and that there is no source in any of the other three loops.

The function $Ym1$ then calculates the magnitude of the current I_1 over the same range of frequencies employed in creating the graphs of Figure 4. The function $Ym2$ does the same for the magnitude of the current I_2 .

It was now possible to display the output of the simulation on the same pair of graphs as that used to record the test results. The results were encouraging, in that the shapes of the curves were similar. But there was a significant discrepancy in the values of the peak frequencies and in the amplitudes of the curves. However, by making incremental changes to the inductors and capacitors assigned to those of Figure 5a at the start of the worksheet and re-running the program, it became possible to establish the correlation illustrated by Figure 7.

Differential-mode current is defined as a flow along the send conductor and back via the return conductor. Figure 7a illustrates the response of this current at the near end of the cable. There are two peaks. The first is at the half-wave frequency, $fh = 6.93$ MHz. The second is at 10.41 MHz. This second peak is due to the interaction with the common-mode loop.

Current in the common-mode loop is defined as a flow along the send conductor and back via the ground conductor. This peaks at 10.26 MHz, the half-wave frequency. This is much higher than that of the differential-mode loop since the relative permittivity is much less. The relative permittivity of the differential-mode loop is higher because the material between the send and return conductors is solid insulation, as illustrated by Figure 1. Most of the insulation in the common mode loop is air.

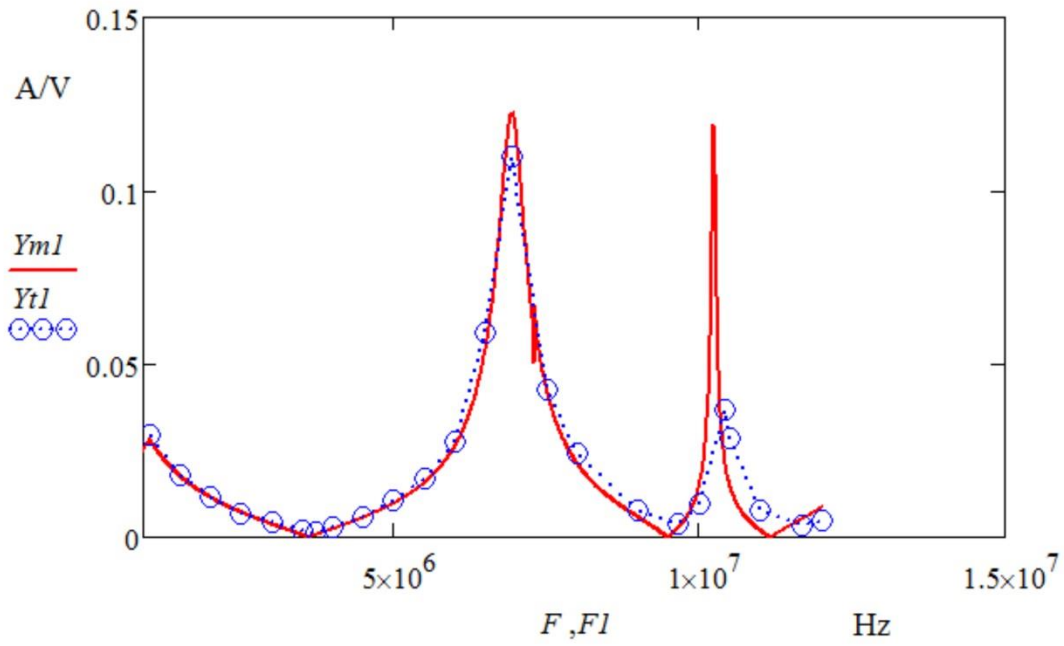
$$Zbranch(f) := \left| \begin{array}{l} \omega \leftarrow 2 \cdot \pi \cdot f \\ \text{for } i \in 1..3 \\ \left| \begin{array}{l} \theta \leftarrow \sqrt{(Rc_i + j \cdot \omega \cdot Lc_i) \cdot (Gc_i + j \cdot \omega \cdot Cc_i)} \\ Z_o \leftarrow \sqrt{\frac{Rc_i + j \cdot \omega \cdot Lc_i}{Gc_i + j \cdot \omega \cdot Cc_i}} \\ Zh_i \leftarrow Z_o \cdot \tanh\left(\frac{\theta}{2}\right) \\ Zv_i \leftarrow Z_o \cdot \operatorname{csch}(\theta) \end{array} \right. \\ (Zh \ Zv) \end{array} \right.$$

$$Zloop(f) := \left| \begin{array}{l} (Zh \ Zv) \leftarrow Zbranch(f) \\ Z11 \leftarrow Rn_1 + Zh_1 + Zv_1 + Zv_2 + Zh_2 + Rn_2 \\ Z12 \leftarrow -(Zh_2 + Zv_2 + Rn_2) \\ Z13 \leftarrow -(Zv_1 + Zv_2) \\ Z14 \leftarrow Zv_2 \\ Z22 \leftarrow Rn_2 + Zh_2 + Zv_2 + Zv_3 + Zh_3 + Rn_3 \\ Z23 \leftarrow Zv_2 \\ Z24 \leftarrow -(Zv_2 + Zv_3) \\ Z33 \leftarrow Rf_2 + Zh_2 + Zv_2 + Zv_1 + Zh_1 + Rf_1 \\ Z34 \leftarrow -(Zh_2 + Zv_2 + Rf_2) \\ Z44 \leftarrow Rf_3 + Zh_3 + Zv_3 + Zv_2 + Zh_2 + Rf_2 \\ \left(\begin{array}{cccc} Z11 & Z12 & Z13 & Z14 \\ Z12 & Z22 & Z23 & Z24 \\ Z13 & Z23 & Z33 & Z34 \\ Z14 & Z24 & Z34 & Z44 \end{array} \right) \end{array} \right.$$

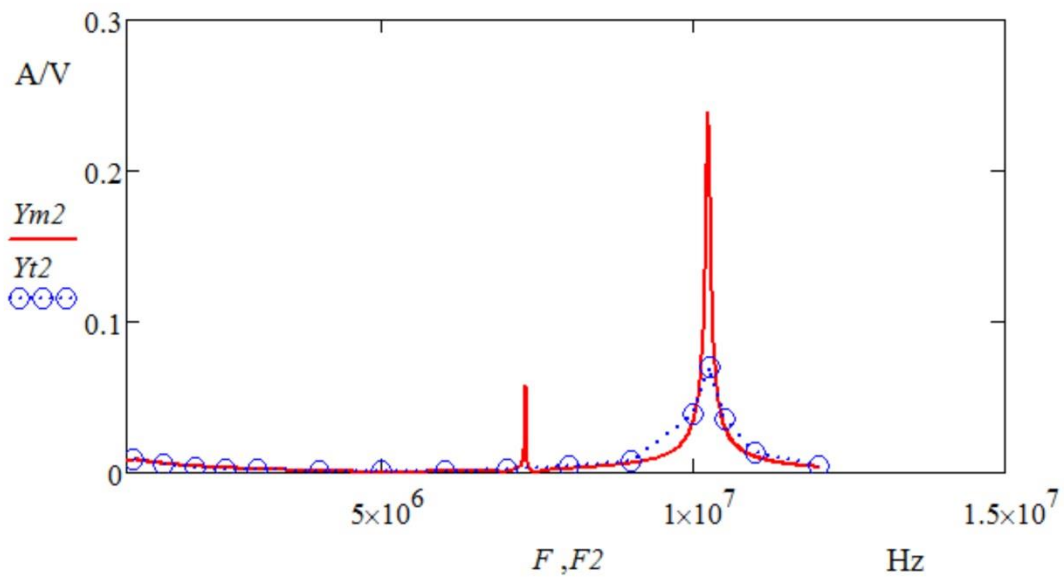
$$i := 100..1200 \quad F_i := i \cdot 10^4 \quad V := \begin{pmatrix} 1 \\ 0 \\ 0 \\ 0 \end{pmatrix}$$

$$Ym1_i := \left| \begin{array}{l} f \leftarrow F_i \\ Z \leftarrow Zloop(f) \\ I \leftarrow \operatorname{lsolve}(Z, V) \\ |I_1| \end{array} \right. \quad Ym2_i := \left| \begin{array}{l} f \leftarrow F_i \\ Z \leftarrow Zloop(f) \\ I \leftarrow \operatorname{lsolve}(Z, V) \\ |I_2| \end{array} \right.$$

Figure 6 Copy of the main page of the Mathcad worksheet



a



b

blue circles: test results. red curve: response of model

Figure 7 Initial correlation between test and model
 a Current in the differential-mode loop conductor
 b Current in common-mode loop

Developing the model

However, there was still a big difference between the amplitude of the peaks recorded by the test results and those derived from the simulation.

The significant feature was that the actual amplitude of the peaks reduced as the frequency increased. So, instead of assuming that the values of the conductances were zero, it was hypothesised that they were significant; and proportional to frequency. Given this assumption, the circuit model of Figure 5a was modified to introduce resistance values in parallel with each capacitor. It was also assumed that the value of each resistance was inversely proportional to the frequency. This led to the relationship:

$$Gc_i = \frac{1}{Re_i} \cdot \frac{f}{fh} \quad (6)$$

Where Re_i is the leakage resistance assigned to conductor i , f is the frequency, and fh is the frequency at which the first peak occurs in Figure 7a

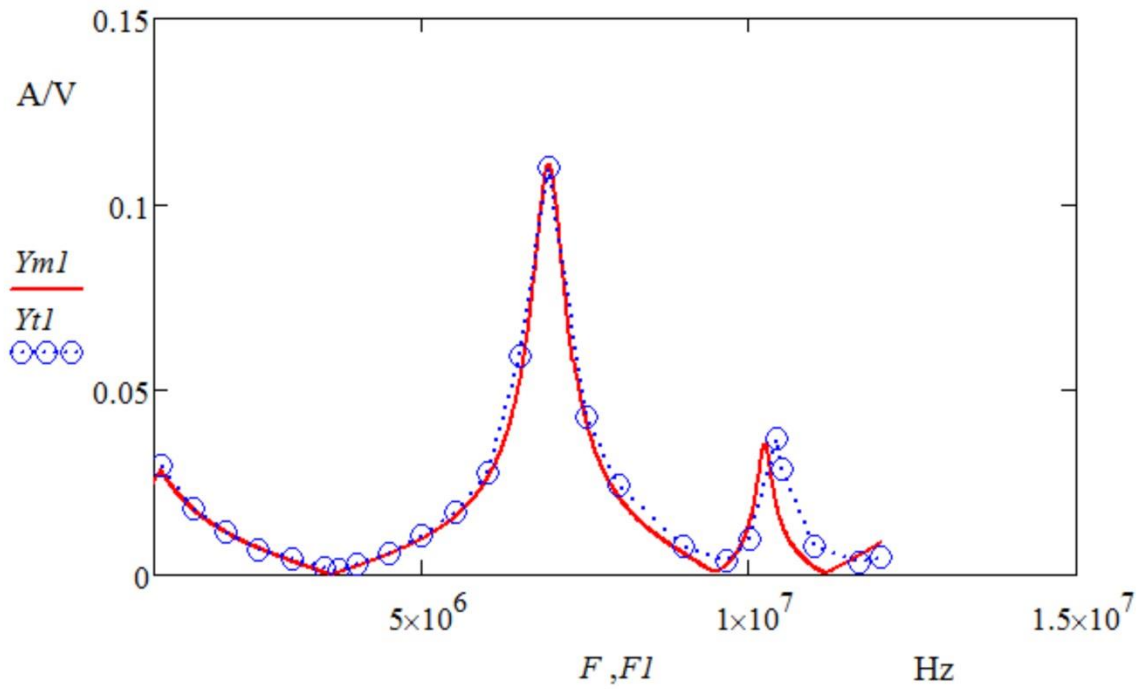
It was a simple matter to modify the worksheet to define the values for these components and include them in the computation. The end result was the graphs illustrated by Figure 8.

The values of the components of the circuit model of Figure 5a could then be defined by displaying the values that had finally been assigned to these variables in the worksheet. There are recorded in the circuit model of Figure 9. This model does not include the circuitry at either interface since the existence of that circuitry has no effect on the coupling between the conductors of the harness.

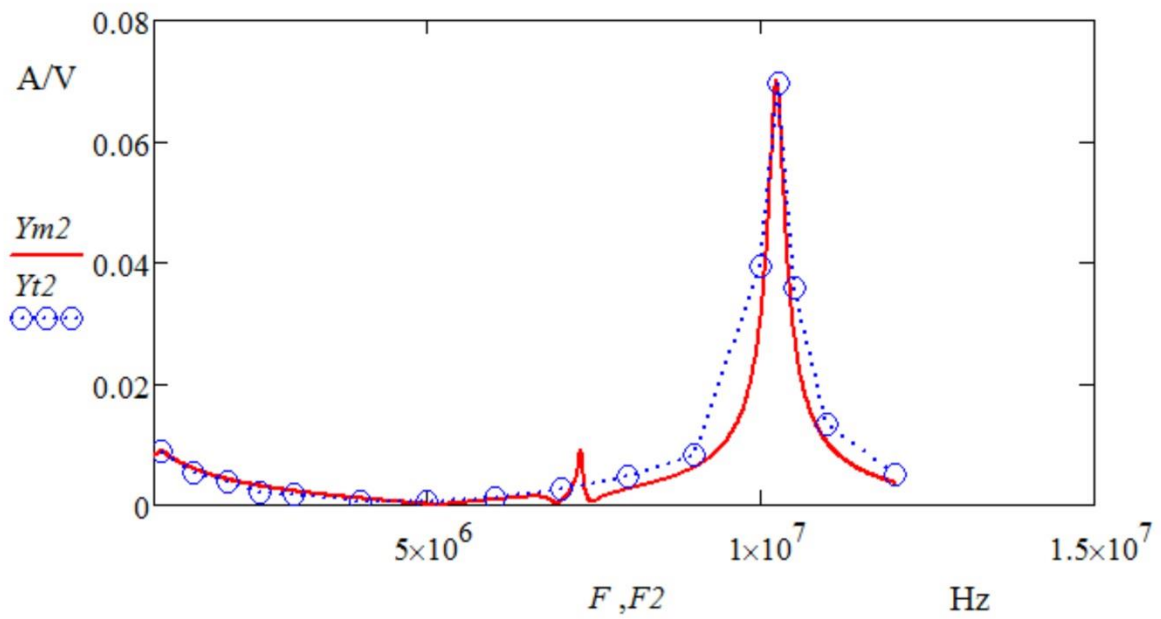
In the setup of Figure 2, the interface at the far end is a short circuit between all three terminals. At the near end, the return conductor is shorted to the ground connection and the send conductor is supplied by a voltage source via a low value resistance. That is, the design of the test equipment is such that there is minimal interaction between the interface circuitry and the assembly-under-test.

The fact that the model of Figure 5b and its relationship with the model of Figure 5a is derived from the equations of Electromagnetic Theory provides credibility to the technique. The fact that close correlation has been achieved between test results and the simulation of the model provides a high degree of confidence in its reliability. The only feature of the model which could be subjected to question is the assignment of values to the resistors Re of equation (6).

The analysis of the dipole antenna shows that the environment can be represented as a 'Radiation Resistor'. So, the concept of assigning a resistor to simulate radiated power is well established, as well as the concept of defining radiated field in terms of current emanating from a conductor.



a



b

blue circles: test results. red curve: response of model

Figure 8 Final correlation between test and model

a Current in send conductor

b Current in ground conductor

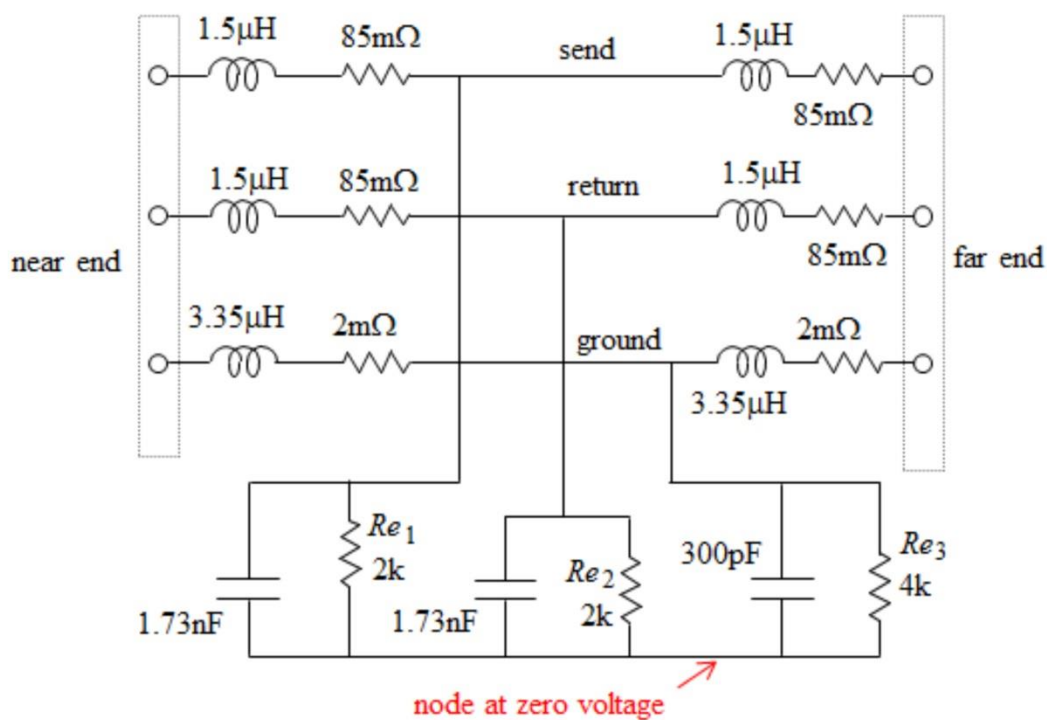


Figure 9 Definitive circuit model of the wiring of the test rig

Under steady state conditions measurement of the insulation of many cables has shown that the resistance is of the order of tens of M-ohms. The only way of reconciling this fact with the existence of radiated power is to assume that any resistor which simulates the environment is a function of frequency.

The facts that a dipole antenna radiates maximum power at the half-wave frequency and that the calculated value of the radiation resistance is a constant indicates that, for a given length of conductor, the amplitude of the radiated current increases in proportion to the frequency. If the frequency applied to a dipole doubles, it will act as two dipoles in parallel. The effective radiation resistance will be halved. Hence equation (6) is entirely plausible.

The fact that the response of the modified model correlates closely with that of the tests on the hardware increases the level of confidence of its credibility and of the reliability of the measurement technique.

In Figure 9, the 2kΩ resistors and the 4kΩ resistor provide an effective indication of the level of radiation emanating from the assembly.

Assessment

Comparing the initial values of equation (3) with the final values of Figure 9 reveals that the value of the inductance of the conductors has changed from 3.17 μH to 3.0 μH . This is probably due to the fact that transient current will tend to flow along the facing surfaces, thus reducing the inductance. The value of the inductance of the copper pipe has reduced from 7.66 μH to 6.7 μH , for the same reason.

Comparing the initial values of equation (4) with the capacitors of Figure 8 reveals that the values of Cc_1 and Cc_2 have increased from 456 pF to 1730 pF. This is because the relative permittivity of the insulation is much higher than unity. The capacitor associated with the copper pipe has reduced from 1890 pF to 300 pF. The probable reason for this is that less current emanating from the structure is arriving back at the cable, because significant current is flowing out into the environment in the form of radiated interference. The resistor Re_3 simulates this radiation.

Conclusion

The fact that there is close correlation between the test results and those of the simulation means that the circuit diagram of Figure 9 provides a reliable model of the interference coupling between the differential-mode loop and the common-mode loop of the signal link. It is possible to add the interface circuitry of the assembly to achieve a complete circuit model of the link. The completed model can then be used to predict the effect of intra-system interference on the performance of the configuration under review.

The first two articles in the series are essentially a reprise of notes copied from a blackboard in Glasgow University in 1959. It is reasonable to assume that any electronic engineer can understand this theory. The tests described in this article can be carried out using general-purpose test equipment. The computations can be handled by software packages that have been available for decades.

Circuit modelling can be used during the design phase of a project to analyse the EMI characteristics of any signal or power link in the system, long before the equipment is submitted to the ministrations of an EMC Test House.